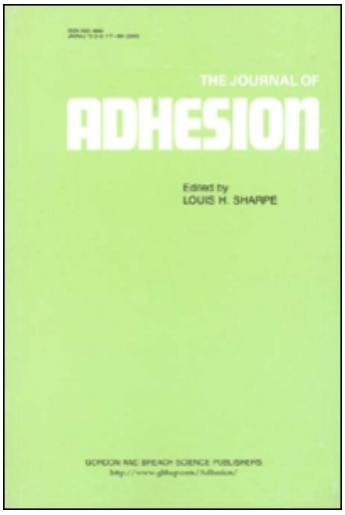

The Journal of Adhesion
Publication details, including instructions for authors and subscription information:
http://www.informaworld.com/smpp/title~content=t713453635

Influence of Experimental Setup and Plastic Deformation on the Shaft-Loaded Blister Test

Emmett P. O'Brien[ab]; Stephanie Goldfarb[c]; Christopher C. White[a]
[a] Buildings and Fire Research Laboratory, National Institute of Standards and Technology, Gaithersburg, Maryland, USA [b] University of Connecticut, Institute of Materials Science, Storrs, Connecticut, USA [c] Department of Mechanical Engineering, Cornell University, Ithaca, New York, USA

To cite this Article O'Brien, Emmett P. , Goldfarb, Stephanie and White, Christopher C.(2005) 'Influence of Experimental Setup and Plastic Deformation on the Shaft-Loaded Blister Test', The Journal of Adhesion, 81: 6, 599 — 621
To link to this Article: DOI: 10.1080/00218460590954601
URL: http://dx.doi.org/10.1080/00218460590954601

The Journal of Adhesion, 81:599–621, 2005

ISSN: 0021-8464 print/1545-5823 online
DOI: 10.1080/00218460590954601

Taylor & Francis
Taylor & Francis Group

Influence of Experimental Setup and Plastic Deformation on the Shaft-Loaded Blister Test

Emmett P. O'Brien
National Institute of Standards and Technology, Buildings and Fire Research Laboratory, Gaithersburg, Maryland, USA and University of Connecticut, Institute of Materials Science, Storrs, Connecticut, USA

Stephanie Goldfarb
Cornell University, Department of Mechanical Engineering, Ithaca, New York, USA

Christopher C. White
National Institute of Standards and Technology, Buildings and Fire Research Laboratory, Gaithersburg, Maryland, USA

In the shaft-loaded blister test (SLBT), plastic deformation often occurs at the contact area between the shaft tip and adhesive layer, leading to a larger displacement (blister height) than if the film was loaded elastically. As a consequence, incorporating the displacement variable into the analysis can result in misleading values of the applied strain energy-release rate, $\mathcal{G}$. In this work, the influence of plastic yielding at the contact area on $\mathcal{G}$ of a thin film was investigated as a function of some common SLBT experimental variables, namely, substrate hole diameter, film thickness, and shaft-tip diameter. Test specimens consisted of plies of pressure-sensitive adhesive tape adhered to a rigid glass substrate. $\mathcal{G}$ was calculated from the following equations: (1) load-based, (2) hybrid, (3) displacement-based, and (4) combination. Decreasing the film thickness, increasing the hole diameter, or decreasing the shaft-tip diameter lead to more plastic yielding at the contact area as well as to an increase in blister height. The increased blister height resulting from plastic deformation leads to disagreement among the values of $\mathcal{G}$ calculated from the different equations when the displacement variable was included in the calculation. However, the load-based equation, which does not include the displacement, was determined to be independent of plastic yielding and the "correct" equation for calculating $\mathcal{G}$. In addition, the film tensile rigidity (Eh) was calculated using an experimental compliance calibration. The effects of film thickness

Received 4 January 2005; in final form 18 February 2005.
Address correspondence to Emmett P. O'Brien, National Institute of Standards and Technology, Buildings and Fire Research Laboratory, 100 Bureau Drive, Bldg. 226, Rm. B350, Gaithersburg, MD 20899-8615, USA. E-mail: emmett.obrien@nist.gov

on the mechanical behavior of the film (bending plate vs. stretching membrane) as well as methods to determine the displacement resulting from plastic deformation are also discussed.

Keywords: Pressure sensitive adhesive tapes; Coatings; Fracture; Yielding; Thin film; Membrane; Bending plate; Bulge test; Point load; Sphere; Contact radius

INTRODUCTION

Plastic deformation complicates testing adhesive joints and coatings by invalidating the assumptions of linear elasticity, consuming energy which is difficult to account for, and causing inelastic strains that can lead to adhesive rupture. Coatings are particularly susceptible to plastic deformation or yielding because of the large stresses generated in the film during testing, which is a consequence of the small cross-sectional area (thinness) and strong adhesion [1]. Recently, the shaft-loaded blister test (SLBT) has been developed to measure the adhesion [2–9] as well as the mechanical properties of thin films and coatings [2, 6, 10–15]. In this experiment, a spherically capped shaft applies a central load to a film, which results in a deflection and delamination (Figure 1). These blister-test geometry experiments and analysis have also recently been adopted for measuring the mechanical response of films using a flat punch in a variety of applications [13,16–21]. The strain energy-release rate, $\mathcal{G}$,

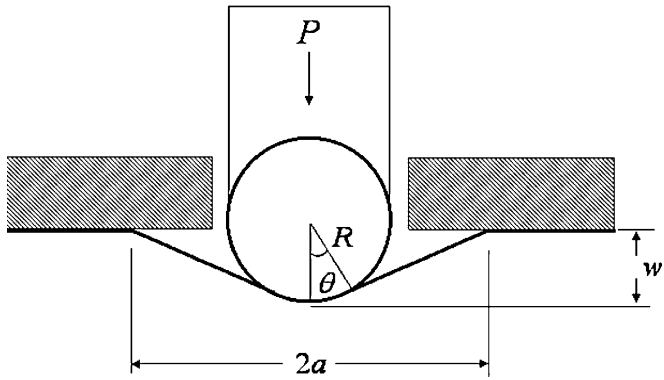

FIGURE 1 Schematic of the shaft-loaded blister test. P is the load, w is the displacement or blister height, a is the blister radius, R is the radius of the shaft tip, and θ is the half angle subtended from the shaft tip.

can be calculated from the following expressions, which were derived using linear elasticity [6]:

$$\mathcal{G} = \left(\frac{1}{16\pi^4 Eh}\right)^{1/3}\left(\frac{P}{a}\right)^{4/3} \quad \text{load-based equation,} \tag{1}$$

$$\mathcal{G} = \frac{1}{\pi^2 Eh}\left(\frac{P}{w}\right)^2 \quad \text{hybrid equation,} \tag{2}$$

and

$$\mathcal{G} = \frac{Eh}{16}\left(\frac{w}{a}\right)^4 \quad \text{displacement-based equation,} \tag{3}$$

where P is the applied load, a is the debond radius, w is the displacement or blister height, E is Young's modulus of the adhesive film, and h is the film thickness. The value of $\mathcal{G}$ calculated from Equation (1) depends strongly on the load, and the value of $\mathcal{G}$ calculated from Equation (3) depends strongly on the displacement. Equation 2 is a combination of Equations (1) and (3). Therefore Equations (1), (2), and (3) are referred to as the load-based, hybrid, and displacement-based equations, respectively. Combining any two of Equations (1), (2), or (3) reveals a fourth equation, denoted as the combination equation, which is identical to that derived by Williams [22] and Jensen [23] and does not incorporate the stiffness (Eh) of the film:

$$\mathcal{G} = \frac{1}{4\pi}\frac{Pw}{a^2} \quad \text{combination equation.} \tag{4}$$

The linear elastic equations for a stretching membrane predict the following constitutive relation [6, 10]:

$$Pa^2 = \left(\frac{\pi Eh}{4}\right)w^3 \tag{5}$$

where, collectively, Eh is known as the film's tensile rigidity, which defines the film's stiffness. The value of Eh of the adhesive layer can be calculated from a compliance calibration where a graph of pa^2 as a function of w^3 yields a slope equal to $(\pi Eh)/4$.

Previous work on the SLBT has shown that significant plastic deformation inevitably occurs at the contact area between the shaft tip and the adhesive film (Figure 2) [2, 6, 9, 10]. As a consequence, the blister height or displacement is overestimated (relative to the elastic model), leading to disagreement among the values of $\mathcal{G}$ if the displacement value is incorporated into the calculation [Equations (2), (3), and (4)]. Wan and

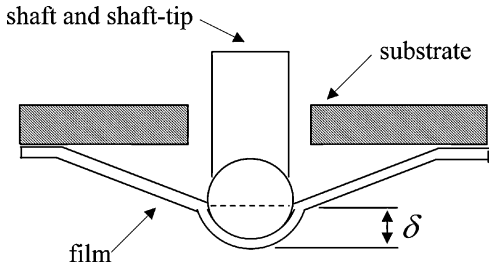

FIGURE 2 Schematic of the area of plastic deformation at the contact area between the shaft tip and the film. The δ symbol is the penetration of the sphere into the film or displacement resulting from plastic deformation.

Mai derived expressions to calculate $\mathcal{G}$ that account for plastic deformation at the contact area [6]. However, this increased complexity was found to be unnecessary if $\mathcal{G}$ was calculated from the load-based equation, which does not incorporate the displacement value and is believed to be independent of plastic deformation at the contact area [2]. For clarity and convenience, we discuss why the load-based equation is believed to be independent of plastic deformation. More details can be found in the work by O'Brien *et al*. [2]. In that work, $\mathcal{G}$ was measured for stacked layers of pressure-sensitive adhesive tape (PSAT) adhered to aluminum. It was argued that if plastic deformation is confined to the area of the shaft tip, and linear elasticity is valid at the crack front (*i.e.*, the yield stress in the peel arm was not exceeded), then it can be assumed that the load and blister radius are in equilibrium. As a consequence, the assumption of linear elasticity and the application of the load-based equation are valid. Therefore, the value of $\mathcal{G}$ calculated from the load-based equation is "correct" despite the presence of plastic deformation at the contact area. The arguments are supported by consistency of the values of $\mathcal{G}$ calculated from the load-based equation for the different stacked layers of PSAT. The work presented in this article further supports the argument.

As just mentioned, if the stress at the crack front is greater than the yield stress of the film or if the size of the plastic zone at the crack tip is greater than or equal to the film thickness, the linear elastic expressions for $\mathcal{G}$ are inapplicable. Equation (6) can be used to calculate the effective membrane stress (for a point load configuration) and can, therefore, be used to determine if elasticity at the crack front is a good assumption [6]:

$$N_{\text{eff}} = (\mathcal{G}Eh)^{1/2}\,[(\log a/r)^2 + 3/4]^{1/2}, \tag{6}$$

where r is the radial distance from the center of the blister. If the stress exceeds the product of the yield stress, σ_y, and the film thickness, h, then

yielding can occur ($N_{\mathrm{Max}} \geq \sigma_y h$). Additional, but more complex, equations for the membrane stress can be found in the work of Wan and Liao [10].

The shaft-tip diameter defines the contact area and, thus, the stress in the film. Wan and Liao found that the maximum membrane stress, N_{Max}, can be expressed as [10]:

$$N_{\mathrm{Max}} = \frac{P}{2\pi R \sin^2 \theta} \quad , \tag{7}$$

where R is the radius of the shaft tip and θ is the half angle that extends from the contact area to the center of the shaft tip (Figure 1). As a result, a smaller shaft-tip diameter or a thinner film is expected to result in more plastic deformation and to overestimate displacement.

In this work, the influence of plastic deformation at the contact area on the SLBT is explored by varying the substrate hole diameter, film thickness, and shaft-tip diameter. The substrate hole diameter is a test parameter chosen by the experimenter and deserves exploration, despite the fact that for linear elastic conditions the size of the initial debond should not matter. More specifically, the applied load, P, debond radius, a, and displacement or blister height, w, are measured and used to calculate $\mathcal{G}$ using four equations: (1) load-based, (2) hybrid, (3) displacement-based, and (4) combination. With the sole exception of the load-based equation, each equation incorporates the displacement value and is sensitive to the treatment of plastic deformation. In addition, the film tensile rigidity (Eh) was calculated using an experimental compliance calibration. The effects of film thickness on the mechanical behavior of the film (bending plate *vs.* stretching membrane) as well as methods to determine the displacement resulting from plastic deformation are also discussed. Test specimens consisted of PSAT, up to three layers thick, adhered to a rigid glass surface.

EXPERIMENTAL[‡]

The adhesive tested in this work was Kapton PSAT, consisting of a silicone-based thermosetting adhesive of thickness 38.1 μm (1.5 mil), covered by a Kapton backing of thickness 25.4 μm (1 mil). The soda lime glass substrate was 9.6 mm thick and was cleaned with acetone prior to

[‡]Certain commercial equipment and materials are identified in this paper to adequately specify the experimental procedure. In no case does such identification imply recommendations by the National Institute of Standards and Technology nor does it imply that the material or equipment identified is necessarily the best available for this purpose.

each application of the tape. Three different hole diameters were investigated: 6.7, 9.8, and 12.9 mm, denoted as small, medium, and large, respectively. To vary the thickness of the film, n stacked plies of PSAT were used, up to $n = 3$. The Young's modulus of the Kapton tape is roughly 3.1 ± 0.1 GPa. In the calculation of the film stiffness, Eh, the stiffness of the backing dominates and the soft adhesive layer was ignored. The bonded PSA dimensions were $25.4 \times 25.4\,\text{mm}^2$.

Experiments were performed on a Universal testing machine (UTM), which measured displacement and load, at a cross-head displacement rate of 0.1 mm/s. Steel ball bearings were used as the shaft tip and were fastened to a steel shaft with a two-part epoxy adhesive. The shaft was attached to a 100-kg load cell *via* a modified drill chuck. Three different shaft-tip diameters were investigated, denoted as small, medium, and large: 3.2, 6.4, and 9.5 mm, respectively. During the experiment, the image of the propagating blister debond was measured using a digital video camera. Note that a fine powder (or other nonstick layer) can be placed between the film and shaft tip to reduce adhesion at the contact area.

Uncertainty in the calculated value of $\mathcal{G}$ is introduced by the value of the blister radius, which is calculated from half the average of the blister diameter in the x and y directions of the video image. The value of the blister radius is affected by any asymmetry of the blister shape and the measurement from the video image. Asymmetry between the x and y direction was generally small (0.1 mm to 0.2 mm) and was likely caused by residual stress [24], anisotropy in the Kapton backing [25], and any heterogeneities in the intrinsic interfacial adhesive toughness. The uncertainty in the value of $\mathcal{G}$ attributable to the blister-radius measurement depends on the magnitude of the value of $\mathcal{G}$ and the equation. For the load-based equation and values of $\mathcal{G}$ observed in this work ranging between 20 and $50\,\text{J/m}^2$, the uncertainty is ± 1 to $2\,\text{J/m}^2$. For the displacement-based equation and $\mathcal{G}$ values between 80 and $130\,\text{J/m}^2$, the uncertainty is ± 10 to $12\,\text{J/m}^2$. For the combination equation and $\mathcal{G}$ values between 35 and $45\,\text{J/m}^2$, the uncertainty is ± 1 to $2\,\text{J/m}^2$. For all experiments, the standard deviation resulting from the sample to sample variation is equal to or more than the uncertainty introduced by the blister radius.

RESULTS AND DISCUSSION

Effects of Varied Substrate Hole Diameter Size on $\mathcal{G}$

The values of $\mathcal{G}$ as a function of the initial substrate hole size were calculated for a single ply and the medium-size ball bearing (6.4-mm

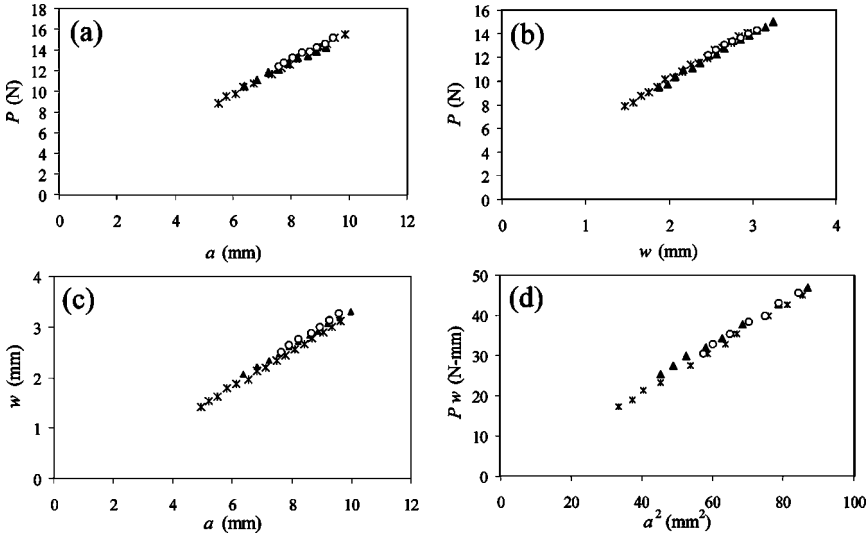

FIGURE 3 Adhesion results for varied initial hole size: (a) load as a function of blister radius, (b) load as a function of displacement, (c) displacement as a function of blister radius, and (d) load displacement as a function of blister radius squared. Symbols are (×) small diameter, (▲) medium diameter, and (○) large diameter.

diameter). The average values for the data sets gathered from these measurements are shown in Figure 3a–d (for clarity, error bars are not shown). From the slopes of these plots (a–d), the value of $\mathcal{G}$ can be calculated from the load-based, hybrid, displacement-based, and combination equations, respectively. The average values of $\mathcal{G}$ and single standard deviation are listed in Table 1. The average and standard deviation are calculated from the values of $\mathcal{G}$ obtained from eight samples.

Table 1 shows that the calculated value of $\mathcal{G}$ depends on which equation was utilized. This observation is consistent with most shaft-loaded blister test experiments and results, probably because of the always-present plastic yielding at the contact area [2, 6, 9, 10]. As discussed in the experimental section, previous work has shown that, for a Kapton PSAT bonded to aluminum, the load-based equation is not only independent of plastic deformation at the contact zone but also agrees well with the value of $\mathcal{G}$ obtained from the pull-off test [2]. Note that the assumption of linear elasticity at the debond front is valid because the effective membrane stress N_{eff} [Equation (5)] is well below the yield stress of the backing. This suggests that the load-based

TABLE 1 Applied Strain Energy Release Rate, $\mathcal{G}$, (J/m^2) Determined from the Equations as a Function of the Blister Hole Size

Size	Load	Hybrid	Displacement	Combination
Small	32.3 ± 2.2	22.4 ± 1.4	85.0 ± 6.6	40.2 ± 2.0
Medium	30.8 ± 0.7	18.5 ± 3.0	94.4 ± 31.3	39.6 ± 3.5
Large	29.8 ± 4.3	15.6 ± 1.6	127.0 ± 30.8	42.6 ± 2.3

Note: The mean $\pm$ one standard deviation about the mean is shown.

equation [Equation (1)] is the most "correct" and preferred of Equations (1) to (4). Table 1 shows that the value of $\mathcal{G}$ calculated from the hybrid equation is smaller, and the values calculated from the displacement-based and combination equation are larger, than the "correct" value of $\mathcal{G}$ determined from the load-based equation. Under ideal linear elastic conditions, the value of $\mathcal{G}$ should be the same for every equation, but the dependence of the calculated $\mathcal{G}$ on displacement determines the sensitivity to the "overestimated" displacement (relative to the elastic case). For instance, in the displacement-based equation, because the value of displacement is in the numerator and is raised to the fourth power ($\mathcal{G} \sim w^4$), the $\mathcal{G}$ is much greater than the load-based equation where displacement is not used in the calculation.

Although Figure 3 reveals substrate hole size has no significant influence on the measured parameters (P, w, a) over the size range studied, Table 1 shows that the hole size can influence the calculated value of $\mathcal{G}$ when the displacement is incorporated into the equation. As the hole size increases, the calculated $\mathcal{G}$ decreases and increases for the hybrid and displacement-based equations, respectively. This suggests that as the substrate hole size increases, the displacement or blister height increases, presumably because of an increase in plastic deformation at the contact zone. The calculated value of $\mathcal{G}$ was not affected by hole size when using the load-based equation, which is expected given the independence on yielding at the contact zone. Calculations based on the combination equation were also independent of hole size.

Effects of Varied Shaft-Tip Diameter Size and Film Thickness on $\mathcal{G}$

Figures 4, 5, and 6 show, for $n = 1$, the effects of shaft-tip diameter on the measured load, displacement, and blister radius. Graphs of the data sets for $n = 1$ and 3 are not shown, because the same trends were

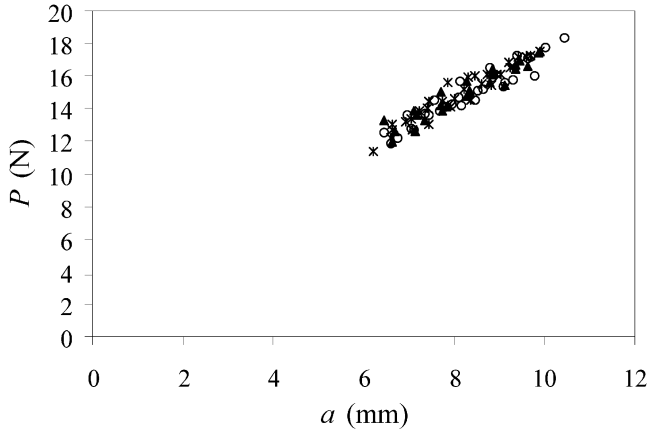

FIGURE 4 The load as a function of blister radius for $n = 1$ and varied shaft-tip diameter. Symbols are (∗) small diameter, (▲) medium diameter, and (○) large diameter.

observed as for $n = 1$. Figure 4 shows the load as a function of blister radius for $n = 1$ for a variety of shaft-tip diameters. All curves appear to overlap. The graph shows that the relationship between the load and debond radius is unaffected by the shaft-tip diameter, which supports the principle that the load-based equation is independent of

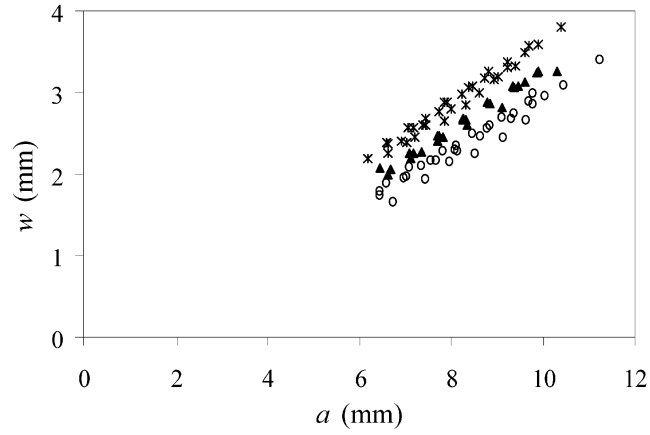

FIGURE 5 The displacement as a function of blister radius for $n = 1$ and varied shaft-tip diameter. Symbols are (∗) small diameter, (▲) medium diameter, and (○) large diameter.

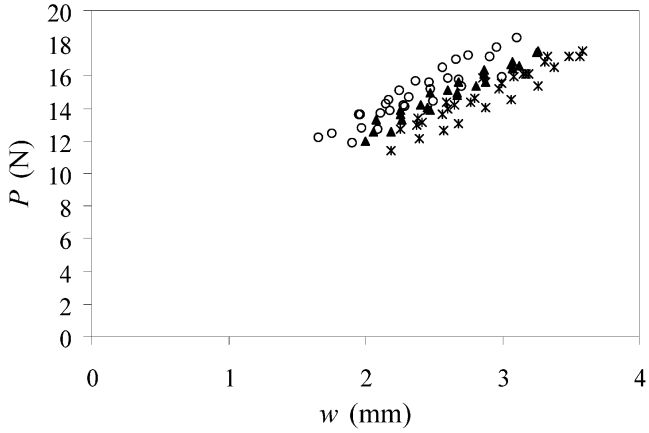

FIGURE 6 The load as a function of displacement for $n = 1$ and varied shaft-tip diameter. Symbols are (∗) small diameter, (▲) medium diameter, and (○) large diameter.

plastic deformation at the contact area. Figure 5 shows the displacement as a function of blister radius for $n = 1$ and varied shaft-tip diameters. The graph shows that as the shaft-tip diameter decreases, displacement increases, presumably because of an increase in plastic deformation at the contact zone. Figure 6 shows the load as a function of displacement for $n = 1$ and varied shaft-tip diameter. This graph shows the expected trend: that increasing the shaft-tip diameter increases the applied loads for a given displacement [10, 14].

The effects of varying the film thickness are shown in Figures 7 and 8. Figure 7 shows the load as a function of blister radius for different values of n and for all shaft-tip diameters. Figure 8 shows the displacement as a function of blister radius for different values of n and the smallest shaft-tip diameter. Figures 7 and 8 illustrate that increasing the film stiffness (n) increases the applied load, but reduces the displacement and overall reduces plastic yielding. In this case, the increase in load and reduced displacement is due to the increase in available stored elastic energy. In addition, Figure 7 again shows that the load-displacement curves are independent of the plastic deformation at the contact area.

Figures 4–8 show that the relationships among P, w, and a change as a function of the shaft-tip diameter and film thickness, but the question remains whether $\mathcal{G}$ is also affected. Tables 2, 3, and 4 list the calculated values of $\mathcal{G}$ as a function of film thickness and shaft-tip diameter for $n = 1$, 2, and 3, respectively. The average and

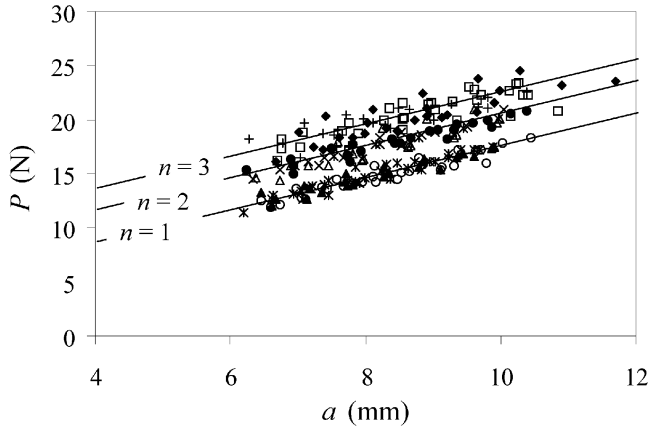

FIGURE 7 The load as a function of blister radius for different values of n. Data sets from all three shaft-tip sizes are shown. Lines are drawn by hand to aid the eye.

standard deviation were calculated from seven samples each. The expected trend was observed in Table 2 for $n = 1$, where decreasing the shaft-tip diameter increased the yielding at the contact area and affected calculations of $\mathcal{G}$ that incorporated the displacement in the equation. As seen in the study of the effect of the substrate hole size

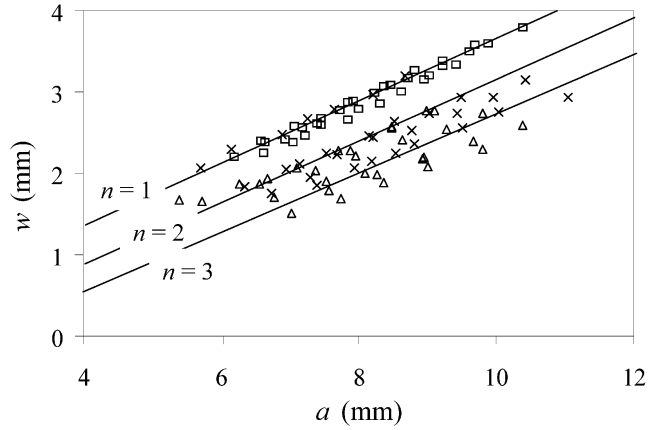

FIGURE 8 The displacement as a function of blister radius for different values of n. Data sets from the smallest shaft-tip size are shown. Lines are drawn by hand to aid the eye.

TABLE 2 Applied Strain Energy Release Rate, $\mathcal{G}$, (J/m^2) Determined from the Equations as a Function of the Shaft-Tip Diameter for $n = 1$

$n = 1$	Load	Hybrid	Displacement	Combination
Small	34.1 ± 2.2	17.7 ± 2.0	123.4 ± 14.8	46.8 ± 7.4
Medium	34.1 ± 4.6	21.3 ± 2.5	83.5 ± 22.9	34.3 ± 3.8
Large	32.9 ± 3.7	25.0 ± 3.9	57.6 ± 3.9	40.4 ± 3.2

Note: The mean $\pm$ one standard deviation about the mean is shown.

TABLE 3 Applied Strain Energy Release Rate, $\mathcal{G}$, (J/m^2) Determined from the Equations as a Function of the Shaft-Tip Diameter for $n = 2$

$n = 2$	Load	Hybrid	Displacement	Combination
Small	28.3 ± 2.0	16.9 ± 5.1	92.2 ± 59.6	48.2 ± 11.2
Medium	25.2 ± 3.9	16.7 ± 4.3	56.4 ± 10.8	38.3 ± 5.0
Large	25.5 ± 5.1	17.3 ± 3.4	59.8 ± 11.4	36.8 ± 3.1

Note: The mean $\pm$ one standard deviation about the mean is shown.

(Table 1), the consistent trend was that values of $\mathcal{G}$ calculated from the hybrid, displacement, and combination were lower, much greater, and greater, respectively, relative to the "correct" load-based equation. The only exception was for the $n = 1$ medium-size shaft tip, where the values of $\mathcal{G}$ between the load-based equation and combination equation were equal.

The effects of the shaft-tip diameter and yielding are most apparent for the thinnest film ($n = 1$) (Table 2) and between the smallest and largest shaft-tip size. As the shaft-tip diameter increased, the values of $\mathcal{G}$ calculated from the load-based equation remain constant, whereas they decreased for the hybrid equation, increased for the displacement-based equation, and exhibited no trend for the combination

TABLE 4 Applied Strain Energy Release Rate, $\mathcal{G}$, (J/m^2) Determined from the Equations as a Function of the Shaft-Tip diameter for $n = 3$

$n = 3$	Load	Hybrid	Displacement	Combination
Small	24.3 ± 5.9	11.7 ± 2.7	94.7 ± 43.7	42.2 ± 19.2
Medium	22.8 ± 5.0	13.8 ± 4.7	56.5 ± 8.8	35.2 ± 9.8
Large	22.0 ± 3.7	13.1 ± 3.8	56.7 ± 12.3	35.7 ± 3.1

Note: The mean $\pm$ one standard deviation about the mean is shown.

equation. The size of the shaft-tip diameter does not affect the values of $\mathcal{G}$ calculated from the load-based equation. This supports the idea that the load-based equation is independent of plastic deformation at the contact area and is the most preferred expression to calculate $\mathcal{G}$.

For $n = 1$ and 3, and similar to $n = 1$, the value of $\mathcal{G}$ calculated from the load-based equation is not affected by the shaft-tip diameter. However, increasing the film thickness reduces the value of $\mathcal{G}$ calculated from the load-based equation, presumably because of an increase in the bending moment and a reduction of plastic deformation of the adhesive film. The peel test behaves similarly where stiffening of the peel arm [26] (or an increase in tensile residual stress [27]) can cause a reduction in peel force. The values of $\mathcal{G}$ calculated from the hybrid equation also decrease as the film thickness increases, presumably because of an increase in bending moment. In fact, the reduction in displacement resulting from an increase in n, which would result in an increase of the value calculated from the hybrid equation, is not enough to overwhelm the effects of increased bending moment.

For the hybrid and displacement equations, the influence of the shaft-tip diameter for $n = 2$ and 3 is not as significant as for $n = 1$. For the smallest shaft-tip diameter and $n = 2$ and 3, the average and standard deviation of $\mathcal{G}$ calculated from the displacement and combination equation is significantly greater than in any other condition. This is due to the smallest diameter imparting the most plastic deformation and the dependence of the displacement equation on the value of w to the fourth power. The increase in plastic deformation is observed graphically (Figure 5), where reducing the diameter of the shaft tip leads to larger values of displacement. Also, the smallest shaft-tip diameter leaves the deepest dimple in the center of the blister, indicating plastic deformation. Note that the size of the dimple is reduced as the film thickness increases. Furthermore, the difference in both the values of $\mathcal{G}$ and the graphs is much greater between the small diameter and either the medium or large diameter than the difference between the medium and large diameter. The influence of the small diameter shaft tip on the value of $\mathcal{G}$ calculated from the combination equation suggests that the load-based equation is more preferable than the combination equation.

Varying the shaft-tip diameter and film thickness caused different amounts of plastic deformation, which was evident from the differences in w seen graphically (Figures 5 and 8). However, differences among the values of $\mathcal{G}$ resulting from yielding are small, with the exceptions of $n = 1$ (all sizes) and the smallest shaft-tip size for $n = 2$ and 3. Therefore, we have observed that plastic deformation can influence the calculated value of $\mathcal{G}$ in cases where the film is thin

or the bearing is small. The yield stress, plastic deformation, film thickness, or the size of the shaft tip can be increased to reduce the undesirable effects. However, we see that for $n = 1$ and a large bearing, the effects of plastic deformation are not reduced sufficiently to result in agreement among all four expressions of $\mathcal{G}$.

Calculation of the Film Tensile Rigidity (*Eh*)

The film stiffness or film tensile rigidity (Eh) was calculated using an experimental compliance calibration and Equation (5). These results were compared with the film tensile rigidity calculated from the Young's modulus, determined from a stress-strain experiment in a UTM. Ideally, if linear elasticity holds and Equations (1) to (5) are correct, then the values of Eh determined from the UTM and the compliance calibration should agree. The results for the varied substrate hole size are listed in Table 5. Table 6 lists the calculated values for the varied film thickness and shaft-tip diameter. The values calculated from the stress-strain experiment are 77,500 N/m, 154,900 N/m, and 309,800 N/m for $n = 1$, 2, and 3, respectively.

Examination of Table 5 shows that the calculated film tensile rigidity did not depend on the size of the substrate hole diameter. This was not unexpected given the similarity of the curves shown in Figure 3. However, the calculated film tensile rigidity depended strongly on the size of the shaft-tip diameter (Table 6). The results also show that the values of Eh determined from the UTM and the compliance calibration agreed best for experiments that utilized the largest shaft tip. This is presumably because of the reduction in both plastic deformation and the value of the displacement. In addition, disagreement between the two methods may also be due to the multilayer structure of stacked layers of glassy backing and soft adhesive as well as any anisotropy in the PSAT backing. See Li, Wang, and Thouless for a rigorous treatment of the debonding of layered structures [28].

TABLE 5 Film Tensile Rigidity, Eh, (N/m) Calculated from an Experimental Compliance Calibration and Equation 5

	Small	Medium	Large
$n = 1$	$54{,}000 \pm 5000$	$48{,}000 \pm 4000$	$41{,}000 \pm 3000$

Note: This data set is for $n = 1$ and varied substrate hole diameters (small, medium, and large). The value calculated from the stress-strain experiment for a single ply is 77,500 N/m. The mean $\pm$ one standard deviation about the mean is shown.

TABLE 6 Film Tensile Rigidity, Eh, (N/m) Calculated from an Experimental Compliance Calibration and Equation 5

	Small	Medium	Large
$n = 1$	$45{,}000 \pm 9000$	$58{,}000 \pm 8000$	$83{,}000 \pm 9000$
$n = 2$	$96{,}000 \pm 31{,}000$	$139{,}000 \pm 32{,}000$	$169{,}000 \pm 47{,}000$
$n = 3$	$155{,}000 \pm 25{,}000$	$164{,}000 \pm 98{,}000$	$242{,}000 \pm 28{,}000$

Note: This data set is for $n = 1$, 2, and 3 and the varied shaft-tip diameter (small, medium, and large). The values calculated from the stress-strain experiment and UTM are 77,500 N/m, 154,900 N/m, and 309,800 N/m for $n = 1$, 2, and 3, respectively. The mean $\pm$ one standard deviation about the mean is shown. Note that the values of Eh determined from the UTM and the compliance calibration showed the best agreement for experiments that utilized the larges shaft tip.

Begley and Mackin noted that using a point-load solution to measure the mechanical properties of thin films in a shaft-loaded blister-test geometry resulted in errors and derived anaytical expressions to account for the spherical loading [14]. Wan and Liao also derived expressions to determine the mechanical properties of thin films using the shaft-loaded blister-test geometry and predicted that increasing the size of the shaft-tip diameter will change the constitutive Equation (5) by a factor of Ω_1 [10]:

$$Pa^2 = \left(\frac{\pi Eh}{4}\right)\Omega_1 w^3, \tag{8}$$

where Ω_1 is a parameter that depends on shaft-tip radius, R, contact radius, c, and angle, θ (Figure 1). Therefore, it is expected that plasticity at the shaft tip should result in decreasing the calculated film tensile rigidity. This was observed in this work; however, the decrease in the value of Eh was most likely due to plastic deformation and was not solely due to the spherical contact area.

Previous research showed improved agreement among the values of $\mathcal{G}$ calculated from Equations (1), (2), and (3) when the value of Eh determined from the compliance calibration was utilized in the calculation [2]. This was likely due to the plastic deformation at the contact area and not because the value of Eh determined from the compliance calibration more closely reflects the mechanical behavior of the film under loading conditions encountered in shaft-loaded blister-test geometry. The dependence of the value of Eh on the shaft-tip diameter and, therefore, the amount of plastic deformation, supports this conclusion.

Methods to Calculate the Contact Radius

There are several methods to calculate the contact radius, c, and the penetration of the sphere into the film, δ, at the shaft tip (Figure 2). The contact radius is related to δ by Equation (9) [29]:

$$\delta = c^2/R. \tag{9}$$

In the work of Wan and Liao, the contact radius can be calculated from the following linear elastic expression [10]:

$$c = \left[\frac{3R^3P(1-v)}{\pi Eh}\right]^{1/4}, \tag{10}$$

where v is Poisson's ratio. This expression assumes a small uniform membrane strain.

Begley and Mackin derived an approximate closed-form solution for the contact radius that incorporates the effects of residual stress [14]:

$$c = \sqrt{\sqrt{\left(\frac{3}{2\pi}\right)\left(\frac{P}{EhR} + 6\pi\varepsilon_0\right)} - 3\varepsilon_0}, \tag{11}$$

where ε_0 is the prestrain in the film attributable to residual stress.

Wan and Mai developed an expression for the yielding radius, a_p, that accounted for plastic deformation at the contact area, which can be used to estimate the contact radius ($a_\mathrm{p} \approx \mathrm{c}$) [6]:

$$a_p \approx a \cdot \exp\left[-\left(\alpha \cdot a^{4/3} - \frac{3}{4}\right)^{1/2}\right], \tag{12}$$

where

$$\alpha = \left(\frac{4\pi^2\sigma_p^3h^2}{P^2E}\right)^{2/3} \tag{13}$$

and σ_p is the yield stress of the film determined from a stress-strain experiment.

The actual value of the penetration depth and displacement resulting from plastic deformation are unknown; however, the magnitude was estimated to be about 1 mm from examination of Figures 5 and 8. None of the models discussed previously predict the correct magnitude of the contact radius and penetration depth. This is not unexpected given that models assume elastic deformations (except for the model of Wan and Mai). However, the disagreement between the experimental results and the model of Wan and Mai is likely also

due to how the plasticity is modeled. Unlike linear elasticity, the solutions that incorporate plasticity are not unique. Plastic yielding behavior among polymers can be very different; it may be rate dependent, time dependent, stress hardening, or stress softening, and small variations in behavior can lead to large differences, especially at high strains. Therefore, plasticity models are highly specific and it is not unexpected that the models may not match the experimental data; however, there may be many other systems that do match the model. This suggests that rather than using these models to predict the contact radius, it is best to actually measure the plastic contribution to the blister height. The plastic deformation at the contact area can be measured by loading and unloading the specimen. Just as in a stress-strain experiment, the degree of plastic deformation can be deduced from the difference between the loading–unloading curves for successive loadings of the same specimen. For this PSAT, the loading–unloading process is complicated because the PSAT will reattach upon regaining contact with the substrate. In adhesive systems where the adhesive will not readhere, such as glassy structural adhesives, this approach is possible. However, measuring the amount of plastic deformation may not be necessary if one is only interested in the measuring $\mathcal{G}$ and utilizes the load-based equation.

Effect of Film Thickness and Shaft-Tip Diameter on the Mechanical Behavior (Stretching Membrane vs. Bending Plate)

In a peel-test geometry, the adhesive layer can behave either like a bending plate, a stretching membrane, or a combination of the two. Whether the film behaves like plate or membrane determines which linear elastic equations should be utilized to model the mechanical properties and delamination of the adhesive. If the load is small or if the film is thick or stiff, then bending behavior dominates. If the load is large or if the film is thin or compliant, then stretching behavior dominates [14]. As a consequence, there is a predicted bending to stretching transition when the load is first applied during contact with the shaft, up to when the debond initiates.

There are several methods to determine mechanical behavior of the film. A simple method is to plot the logarithmic load as a function of the logarithmic displacement ($P \propto w^{\gamma}$) during the initial loading of the film prior to debond initiation. The value of the slope, γ, indicates the mechanical behavior, where $\gamma = 1$ is characteristic of a bending plate and a value of $\gamma = 3$ is characteristic of a stretching membrane [10].

In addition, Wan and Liao derived the expressions to determine the normalized membrane stress, $\beta = (N\,a^2/D)^{1/2}$, which indicates the ratio of stretching stress to bending rigidity [10]. N is the film stress and D is the flexural rigidity. A small value of β (less than 0.1) indicates a pure bending plate and a large β (greater than 20) indicates a stretching membrane.

A similar dimensionless parameter was derived by Komaragiri, Begley, and Simmonds to determine if bending can or cannot be ignored (for both pressure loading and point loading) [15]:

$$\lambda = \left[12 \cdot (1 - v^2)\right]^{3/2} \left(\frac{Pa^2}{Eh^4}\right). \tag{14}$$

The value of λ determines if the film behaves more like a bending plate or stretching membrane.

The values of the slope, γ, of the log load as a function of log displacement are listed in Table 7 for the varied substrate hole size. Table 8 lists the values of γ for the varied shaft-tip diameter and film thickness. Tables 7 and 8 show that for this adhesive, the measured value of γ does not depend on the substrate hole size, shaft-tip diameter, and film thickness. This is unexpected given that Wan and Liao showed analytically and experimentally that increasing the shaft-tip diameter results in a larger gradient, γ [10]. However, this work

TABLE 7 Slope, γ, of the Log Load–Log Displacement Curve ($P \propto w^{\gamma}$)

	Small	Medium	Large
$n = 1$	2.3 ± 0.3	2.3 ± 0.4	2.4 ± 0.4

Note: This data set is for $n = 1$, and the varied substrate hole diameter (small, medium, and large). For a pure bending plate, $\gamma = 1$, and for a stretching membrane, $\gamma = 3$. The mean $\pm$ one standard deviation about the mean is shown.

TABLE 8 Slope, γ, of the Log Load–Log Displacement Curve ($P \propto w^{\gamma}$)

	Small	Medium	Large
$n = 1$	2.2 ± 0.3	2.7 ± 0.4	2.3 ± 0.2
$n = 2$	2.3 ± 0.3	2.2 ± 0.3	2.3 ± 0.3
$n = 3$	2.3 ± 0.4	2.4 ± 0.4	2.1 ± 0.2

Note: This data set is for $n = 1$, 2, and 3 and varied shaft-tip diameter (small, medium, and large). For a pure bending plate, $\gamma = 1$, and for a stretching membrane, $\gamma = 3$. The mean $\pm$ one standard deviation about the mean is shown.

agrees with the research of Begley and Martin [14], which showed analytically and experimentally that, for both a point load and spherical load of a stretching membrane, it is expected that $P \propto w^3$. However, the scatter in the data suggests that a UTM, which measures the load and displacement, may be insensitive to the effects of substrate hole diameter, shaft-tip diameter, and film thickness. The values of γ listed in Tables 7 and 8 are roughly 2.3 ± 0.3 for all test conditions, which suggests that the film behaves more like a stretching membrane than a bending plate. The stretching film behavior of this adhesive is supported by calculations using the methods of Wan and Liao, and Komaragiri, Begley, and Simmonds.

Effect of Applying Bending Plate Equations to Calculate $\mathcal{G}$

It is of interest to compare values of $\mathcal{G}$ determined for a bending plate model with the stretching membrane model we have used previously [Equations (1) to (4)]. Note that we have shown previously that the adhesive film behaves more like a stretching membrane ($\gamma = 2.3 \pm 0.3$). Malychev and Salganik derived the load-based, combination and displacement-based equations for a bending plate [30]:

$$\mathcal{G} = \frac{3(1-v^2)}{8\pi^2 E h^3} P^2 \qquad \text{load-based equation,} \tag{15}$$

$$\mathcal{G} = \frac{Pw}{2\pi a^2} \qquad \text{combination equation,} \tag{16}$$

and

$$\mathcal{G} = \frac{2Eh^3}{3(1-v^2)} \frac{w^2}{a^4} \qquad \text{displacement-based equation.} \tag{17}$$

The combination equation [Equation (16)] is identical to that derived by Wan [11] and Williams [22]. For a bending plate, Equations (15) to (17) will be most applicable when the displacement in less than the film thickness [31]. Furthermore, for a bending plate, the load is predicted to be constant during delamination. In these experimental results, the displacement is much greater than the film thickness and the load is not constant. Therefore, the membrane equations are more appropriate for the adhesive system investigated in this work.

The strain energy-release rate calculated from Equation (16) varies by as much as five orders of magnitude from the load-based stretching membrane equation [Equation (1)]. Note that this difference is significantly reduced as the film thickness increases. The combination

equation derived for a bending plate [(Equation 16)], which does not incorporate the mechanical properties of the film, differs by a factor of two from the membrane solution of the combination equation [(Equation 4)]. Therefore, the bending plate equation yields a value of $\mathcal{G}$ twice as large as the membrane solution. The displacement-based equation for the bending plate is also very sensitive to the film thickness. For $n = 1$, the difference between the bending plate and stretching membrane case was less than a factor of two; however, increasing the film thickness increased the difference by as much as four orders of magnitude.

Effect of Shaft-Tip Diameter and Film Thickness on Scaling of Equations (1) to (4)

If Equations (1) to (4) have been derived correctly and the test specimens behaved linear elastically, then the data plotted in Figures 3 to 8 should be linear and should extrapolate back to the origin ($P = 0$, $w = 0$, and $a = 0$). Examination of Figures 3 to 8 reveals three trends. First, graphs of the load as a function of blister radius extrapolate through the origin, which suggests linear elasticity occurs and supports the idea that the load-based equation is independent of the plastic deformation at the contact area. The second trend is that reducing the shaft-tip diameter causes the graphs to extrapolate more closely through the origin. This supports the reasoning that the offset between the extrapolated line and origin is due to the finite width of the shaft tip, which was suggested by Wan and Mai [6]. Lastly, as the film thickness was increased, the extrapolated line tended to pass further from away from the origin.

Practical Implications for the Shaft-loaded Blister Test

This work has practical implications for the design of a SLBT experiment. Wan and Liao proposed that to reduce plastic deformation at the contact area, the radius of the shaft tip should greater than or equal to [10]:

$$R \geq \frac{9P}{2\pi h \sigma_y}, \tag{18}$$

where σ_y is the yield stress of the adhesive film. In other words, one should increase the shaft-tip diameter, reduce the applied load, and increase the thickness to reduce the stress and possibility of yielding in the adhesive film. The present work has shown that plastic

deformation can be reduced by increasing the shaft-tip diameter, despite the expected increase in load. This work has also shown that the size of the shaft tip does not affect the load-based equation and so the size of the shaft tip seems to be unimportant; however, the chance for film rupture can be reduced if a larger shaft tip is utilized and that enables the application of greater loads per given displacements and, therefore, greater strain energy-release rates. Begley also notes that the greater applied loads facilitated by a larger shaft-tip diameter provide better load resolution, which has practical implications for applying atomic force microscopy to adhesion studies and measuring the mechanical properties of thin films [14]. By reducing the stress in the film, a thinner film can be utilized, which will more closely follow the assumption of a thin stretching membrane used to derive the expressions of $\mathcal{G}$. Furthermore, a larger bearing that fits snuggly into the initial blister hole enables the shaft tip and blister to be easily centered and can help to reduce sample to sample scatter.

Plastic deformation may also be influenced by the cross-head displacement rate, which affects the strain rate and, therefore, the yield stress and yield strain in the adhesive layer. Although no experiments have been performed to investigate the effect of displacement rate on plastic deformation at the contact area, effects similar to those presented in this work could be expected. However, for this PSAT, increasing the test rate results in larger values of $\mathcal{G}$ because of increase in the debond velocity and viscoelastic effects in the soft pressure-sensitive adhesive layer. Therefore, deconvolution of the effects of plastic deformation and debond velocity on $\mathcal{G}$ could prove difficult.

CONCLUSIONS

The influence of the film thickness, substrate hole diameter, and shaft-tip diameter on plastic deformation at the contact area and blister height was measured. Increasing the hole size slightly increased the amount of plastic deformation, which was evident from the changes in $\mathcal{G}$, but did not significantly affect the measured P, w, or a. Increasing the film thickness (n) increased the applied load and decreased the displacement. Decreasing the shaft-tip diameter increased the displacement or blister height resulting from plastic deformation at the contact area. The presence of both effects suggests that there are differences in the amount of plastic deformation among the different test conditions. Differences in the calculated values of $\mathcal{G}$ were observed when the displacement was incorporated into the calculation. Relative to the "correct" load-based equation, differences among the equations for $\mathcal{G}$ can be reduced using a large shaft-tip diameter. The value of

$\mathcal{G}$ calculated from the load-based equation decreased slightly as the film thickness increased. This is a trend typically observed in many other adhesive tests. The film tensile rigidity, Eh, calculated from the experimental compliance calibration agreed best with values determined from a tensile test of the film when the largest shaft-tip diameter was used. The contact radius and displacement resulting from plastic deformation should be determined experimentally; however, it may be unnecessary if the load-based equation is utilized. Methods to determine if the film behaves like a bending plate or stretching membrane were discussed. Using these techniques, it was found that the film mostly behaves like a thin stretching membrane. The values of $\mathcal{G}$ were significantly different depending on whether the equations for a bending plate or stretching membrane were used.

ACKNOWLEDGMENTS

Financial support for Stephanie Goldfarb was provided by the National Science Foundation through the Summer Undergraduate Research Fellowship (SURF) program at NIST. The authors thank their colleagues at the National Institute of Standards and Technology: Jason Garver and Ned Embree for their mechanical expertise and Xiaohong Gu, Amanda Forster, Aaron Forster, Peter Drzal, Jon Martin, and Bryan Vogt for providing helpful comments. We also appreciate the help of the editor and the comments by the referees.

REFERENCES

[1] Lai, Y. H. and Dillard, D. A., *J. Adhes. Sci. Technol*. **8**, 663–678 (1994).
[2] O'Brien, E. P., Ward, T. C., Guo, S., and Dillard, D. A., *J. Adhes*. **79**, 69–97 (2003).
[3] Liao, K. and Wan, K. T., *J. Mat. Sci. Lett*. **19**, 57–59 (2000).
[4] Liao, K. and Wan, K. T., *J. Compos Tech. Res.* **23**, 15–20 (2001).
[5] Wan, K. T., DiPrima, A., Ye, L., and Mai, Y. W., *J. Mater. Sci*. **31**, 2109–2116 (1996).
[6] Wan, K. T. and Mai, Y. W., *Int. J. Fract.* **74**, 181–197 (1995).
[7] Wan, K. T. and Mai, Y. W., *Mater. Sci. Res. Int.* **1**, 78–81 (1995).
[8] Xu, X. J., Shearwood, C., and Liao, K., *Thin Solid Films* **424**, 115–119 (2003).
[9] O'Brien, E. P., Case, S. L., and Ward, T. C., *J. Adhes*. **81**, 1–18 (2005).
[10] Wan, K. T. and Liao, K., *Thin Solid Films* **352**, 167–172 (1999).
[11] Wan, K. T., *J. Adhes*. **70**, 209–219 (1999).
[12] Wan, K. T., Guo, S., and Dillard, D. A., *Thin Solid Films* **425**, 150–162 (2003).
[13] Ju, B. F., Liu, K. K., Ling, S. F., and Ng, W. H., *Mech. Mater.* **34**, 749–754 (2002).
[14] Begley, M. R. and Mackin, T. J., *J. Mech. Phys. Solids* **52**, 2005–2023 (2004).
[15] Komaragiri, U., Begley, M. R., and Simmonds, J. G., *J. Appl. Mech*. **72**, (2005) accepted.
[16] Wan, K. T., *J. Adhes*. **75**, 369–380 (2001).
[17] Liu, K. K. and Ju, B. F., *J. Phys. D: Appl. Phys*. **34**, L91–L94 (2001).
[18] Wan, K. T., *J. Appl. Mech. Trans. ASME* **69**, 110–116 (2002).

[19] Wan, K. T. and Dillard, D. A., *J. Adhes*. **79**, 123–140 (2003).
[20] Liu, K. K., Khoo, H. S., and Tseng, F. G., *Rev. Sci. Instrum*. **75**, 524–531 (2004).
[21] Ju, B. F., Wan, K. T., and Liu, K. K., *J. Appl. Phys*. **96**, 6159–6163 (2004).
[22] Williams, J. G., *Int. J. Fract.* **87**, 265–288 (1997).
[23] Jensen, H. M., *Eng. Fract. Mech*. **40**, 475–486 (1991).
[24] Jensen, H. M. and Thouless, M. D., *Int. J. Solids Struct.* **30**, 779–795 (1993).
[25] Park, T., Dillard, D. A., and Ward, T. C., *J. Polym. Sci. Part B: Polym. Phys*. **38**, 3222–3229 (2000).
[26] Kim, J., Kim, K. S., and Kim, Y. H., *J. Adhes. Sci. Technol*. **3**, 175–187 (1989).
[27] Thouless, M. D. and Jensen, H. M., *J. Adhes. Sci. Technol*. **8**, 579–589 (1994).
[28] Li, S., Wang, J., and Thouless, M. D., *J. Mech. Phys. Solids* **52**, 193–214 (2004).
[29] Barquins, M., *Wear* **158**, 97–117 (1992).
[30] Malyshev, B. M. and Salganik, R. L., *Int. J. Fract.* **1**, 114–128 (1965).
[31] Williams, M. L., *J. Appl. Polym. Sci*. **13**, 29–40 (1969).